Title

Hippocampal cells multiplex positive and negative engrams

Authors

Monika Shpokayte[1,5], Olivia McKissick[2], Bingbing Yuan[3], Bahar Rahsepar[4,5], Fernando R. Fernandez[4,5], Evan Ruesch[5,], Stephanie L. Grella[4,5], John A. White[4,5], X. Shawn Liu[6*], Steve Ramirez[4,5*]

Affiliations

[1]Graduate Program for Neuroscience, Boston University, Boston, MA, 02215

[2]Neuroscience Graduate Program, Brown University, Providence, RI, 02912

[3]Whitehead Institute for Biomedical Research, MIT, Cambridge, MA, 02142

[4]Department of Biomedical Engineering, Boston University, Boston, MA, 02215

[5]Department of Psychological and Brain Sciences, The Center for Systems Neuroscience, Neurophotonics Center, and Photonics Center, Boston University, Boston, MA, 02215

[6]Department of Physiology and Cellular Biophysics, Columbia University Medical Center, New York, NY 10032

*Corresponding Author

One sentence summary

The hippocampus contains neurons corresponding to positive and negative engrams, which are segregated by their molecular, cellular, and projection-specific features.

Abstract

The hippocampus is involved in processing a variety of mnemonic computations including the spatiotemporal components, as well as the corresponding emotional dimensions, of contextual memory.[1-3] Recent studies have demonstrated vast structural and functional heterogeneity along the dorsal-ventral axis[4] of the hippocampus, and while much is known about how the dorsal hippocampus processes spatial-temporal content, much less is known about whether or not the ventral hippocampus (vHPC) partitions positive and negative experiences into distinct sets of cells.[4-9] Here, we combine transgenic and all-virus based activity-dependent tagging strategies to visualize multiple valence-specific engrams in the vHPC and demonstrate two partially segregated, albeit physiologically similar, populations that respond to positive and negative experiences. Next, using an RNA Sequencing approach, we find that vHPC positive and negative engram cells display distinct transcriptional programs in which neuroprotective- and neurodegenerative-related gene sets are enriched, respectively. Additionally, while optogenetic manipulation of tagged cell bodies in vHPC is not sufficient to drive behavior, tagged vHPC terminals projecting to the amygdala and nucleus accumbens, but not the prefrontal cortex, have the capacity to drive preference and avoidance when stimulated, as well as to "switch" or "reset" their capacity to drive either, thereby demonstrating their flexible contributions to behavior. We conclude that the vHPC contains genetically, cellularly, and behaviorally distinct populations of cells processing positive and negative memory engrams. Together, our findings provide a novel means by which to visualize multiple engrams within the same brain and point to their unique genetic signatures as putative avenues for future therapeutic interventions.

The brain contains a rich repository of memories that are often imbued with positive and negatively valenced information. These experiences leave enduring structural and functional changes that are parceled up into discrete sets of cells and circuits that comprise memory engrams[10]. Recent studies have successfully visualized and manipulated defined sets of cells previously active during a single experience[9-16], though how multiple engrams of varying valences (hereafter defined as cells that differentially respond to positive or negative events in a stimulus-independent manner[17]) are represented within the same brain region remains poorly understood. As previous studies have suggested that ventral hippocampus (vHPC) in particular demarcates and relays emotional information to various downstream targets, here we sought to characterize the molecular and cellular identities, as well as the behaviorally-relevant functions, of vHPC cells processing positive and negative engrams. Specifically, to address the question of how the vHPC processes multiple emotional experiences, we first devised a strategy combining various cFos-based tagging methods to visualize engrams across three discrete timepoints. Further, we used this strategy to electrophysiologically probe vHPC cells processing positive and negative memories, followed by performing large-scale RNA sequencing to investigate the genetic features of these sets of cells. Finally, we tested the causal role and functional flexibility of such vHPC cells in both a cell body and projection-specific manner.

To access cells across multiple timepoints and in an activity-dependent, within-subject manner, we used the Fos-based transgenic animal, TRAP2[17], under the control of 4-Hydroxy-Tamoxifen (4-OHT) paired with an all-virus Fos-based strategy under the control of doxycycline[10] (Dox; Extended Data Fig. 1). TRAP2 mice expressing iCre-ERT2 recombinase were injected bilaterally with AAV9-Flex-DIO-TdTomato (tdT), enabling us to label active neurons in the vHPC with tdT.

These same mice were also injected with a virus cocktail of AAV- cFos-tTA + AAV-TRE-EYFP, thus yielding two inducible windows for tagging vHPC cells (See methods). The latter approach couples the *c-Fos* promoter to the tetracycline transactivator (tTA), which, in its protein form, directly binds to the tetracycline response element (TRE) in a doxycycline-(Dox)-dependent manner and drives the expression of a protein of interest (i.e. EYFP).

In the first set of experiments, vHPC cells processing positive or negative experiences were tagged with EYFP and tdT, respectively, followed by timed perfusions to capture a third experience reflected by endogenous cFos expression (Fig. 1a). This enbabled us to measure the cellular co-localization of tdT, EYFP, and cFos to infer which cells were active in one or more of the three experiences. Our experimental design utilized four different groups and mice were subjected to three of four experiences to tag cells active during each behavioral epoch: two experiences were negative, namely foot shocks (Shock[10]) and restraint stress (Stress[18]), and two experiences were positive, namely female exposure (Female[18,19]) and condensed milk (Milk[20]). Group 1 mice underwent a Shock-Female-Stress sequence; Group 2 mice underwent a Shock-Shock-Stress sequence; Group 3 mice underwent a Female-Shock-Milk sequence; and lastly, Group Four mice underwent a Female-Female-Milk sequence (Fig. 1b). All mice exhibited a similar proportion of tagged cells across all three tagging approaches regardless of valence (Fig. 1c-e; See Methods). Histological analyses revealed that there were significantly higher rates of cells showing co-localization of tdT, EYFP and c-Fos in mice subjected to three negative or three positive experiences, compared to mice given both positive and negative experiences, and the order in which these behaviors occurred did not have an effect in the total observed overlap counts (Fig.

1f-i, j-m). These findings raise the intriguing possibility that vCA1 designates emotionally-relevant information to two partially non-overlapping sets of cells .

Next, we used the same dual-tagging strategies to characterize the basic physiological properties of vHPC cells (Fig. 2a-c). Interestingly, we did not observe any differences in firing frequency (Fig. 2d), suprathreshold characterization (Fig. e-g), adaptation rate (Fig. 2h), input rate (Fig.. 2i), or spike rates (Fig. 2j-l) suggesting that, despite recruiting partially non-overlapping sets of cells for positive and negative experiences, these tagged cells themselves share similar physiological characteristics. Although we found no functional cellular differences among these cells, we next asked whether or not their molecular composition contained distinct genetic profiles. To catalogue the molecular landscape of vHPC cells, we tagged a positive or negative experience (Fig. 3a) and performed RNA-seq using nuclei isolated by Fluorescence-Activated Cell Sorting (FACS), which showed ~0.6% tagged nuclei from each group (Fig. 3b-d). Negative and positive vCA1 cells showed distinct transcriptomes compared to mock hippocampal neurons (i.e. untagged vHPC cells) as shown by the principal component analysis (PCA; Extended Data Fig. 2a). The top 20 differentially expressed genes (DEGs) identified between negative vs. mock (Extended Data Fig. 2b) and positive vs. mock (Extended Data Fig. 2c) showed no overlap with each group, and Gene Ontology (GO) analysis showed divergent biological processes, cellular components, and molecular functions associated with each group as well (Extended Data Fig. 4 and 5). Among the top 30 DEGs identified between negative and positive cells, 19 genes were expressed at a higher level in the positive engram cells while the expression of the other 11 genes were lower in the positive engram cells when compared to negative engram cells. These data suggest that negative

and positive-tagged cells contain transcriptionally distinct profiles and transcriptomes (Fig. 3d). Overall, these candidate genes will be of great interest for future studies to investigate a potential causal link between the molecular features of positive and negative engram vHPC cells and their corresponding functional outputs.

To gain deeper insight into the molecular signatures of transcriptomes associated with negative and positive vCA1 cells, we next performed a Gene Enrichment Set Analysis (GESA, see methods) using the DEGs between positive and negative vHPC cells. Genes involved in synaptic functions were differentially expressed in these two groups of cells (Fig. 3e), further suggesting that they are molecularly distinct neuronal populations. Remarkably, when we grouped a set of genes with defined neuroprotective functions[21] (Extended Data Table 1) and another set of genes thought to be involved in Alzheimer's Disease (AD) and neurodegeneration[22] (Extended Data Table 2), GESA revealed that the neuroprotective gene set was only enriched and upregulated in positive cells, but not enriched in the negative cells (Extended Data Fig. 3a). In contrast, the AD and neurodegenerative gene set was enriched in negative cells but not in positive cells (Extended Data Fig. 3b). These striking findings point to vHPC-mediated positive and negative engrams as potential therapeutic targets for neurodegeneration diseases and as putative biomarkers for the emergence of neuroprotective phenotypes.

Next, to test for a causal role of tagged vHPC cell bodies in driving behavior, we infused a virus cocktail of AAV9-cFos-tTA and AAV9-TRE-ChR2-EYFP or AAV9-TRE-EYFP (Extended Data Fig. 6a) and implanted an optical fiber bilaterally above the injection site. On Day 1 of the protocol

mice were habituated to a place preference/ avoidance chamber, and we observed similar levels of baseline behavior activity between EYFP- and ChR2-positive animals (Extended Data Fig. 6). On Day 3, the mice were taken off Dox and cells active during a negative or positive experience were tagged in vCA1(Extended Data Fig. 6 c, g). All animals underwent an "induction" protocol: as previously reported[12], in this protocol mice first undergo an optogenetic place preference/avoidance test (Pre-Induction), and are then exposed to an experience of the opposite valence while receiving optical stimulation of the same set of originally tagged cells (Induction), and end in a final optogenetic preference/avoidance test (Post-Induction). Surprisingly, during the pre-induction and post-induction phases, mice did not exhibit preference or avoidance for either side of the chamber (Extended Data Fig. 6c-j). These negative findings raise the question of whether vCA1's role in driving behavior is determined in a terminal-specific manner[23], a notion which dovetails with recent studies suggesting that computations along the axons of a given cell body can differentially drive behavior contingent on the downstream target[7].

Accordingly, because vCA1 has been recently shown to preferentially route content-specific information in a target-specific manner, we tested whether activation of vCA1 outputs could modulate preference and avoidance-related behaviors. Viral injections were targeted in the vCA1 and optic fibers were placed bilaterally over the BLA, NAcc, or PFC (Fig. 4a-b) given their role in organizing various aspects of emotional experiences[7,8,24-27,], and we followed the same induction paradigm as described above (Fig. 4c, e). We first found that all terminals were capable of activating their corresponding downstream targets (Extended Data Fig.7). We then observed that stimulation of vCA1 terminals over the BLA and NAcc was sufficient to drive preference and

avoidance in the respective positive and negative groups (Fig. 4c-f). Notably, these terminals also had the capacity to "switch" or "reset" the behaviors they drove (Fig. 4d,f), and there was no significant difference in distance travelled across all groups during light on or off epochs in an open field (Extended Data Fig. 8). Following the induction protocol, terminals that initially drove preference were now capable of driving avoidance, and those initially driving avoidance returned to driving baseline levels of behavior when stimulated. In contrast, we did not see this effect in the PFC terminals, nor in EYFP controls (Fig. 4c-f). Furthermore we did not observe this effect when the original memory tag was of a neutral homecage environment, nor did the frequency of the stimulation have an effect in driving behavior (Extended Data Fig. 9). Taken together, these results suggest that, despite sharing partially non-overlapping molecular and neuronal signatures, vHPC cell bodies perhaps relay their behaviorally-relevant and valenced content to downstream targets, corroborated by evidence showing that vHPC axonal outputs preferentially route independent features of a given behavior[7].

Here we have shown that the vHPC processes positive and negative experiences in defined populations of cells that are partially distinct at the molecular and cellular levels, as well as in their capacity to drive behaviors through functionally plastic projection-specific terminals. Our immunohistochemical data suggest that vCA1 contains at least three populations of neurons: two subsets which preferentially respond to positive or negative valences, and a population which responds to both, perhaps reflecting a biological predilection for salience.[5] While their exact brain-wide structural and functional outputs remain undetermined, we speculate that our observed population of vCA1 cells responding to fear are a superset of recently observed anxiety cells that

transmit information to the hypothalamus[26] and PFC[27], and that vCA1 cells processing fear and/or reward perhaps route information to and innervate the BLA and NAcc at differing anatomic, receptor- and cell-type specific loci, thus optimizing their capacity to integrate mnemonic information[26].

Additionally, by combining transgenic activity-dependent tagging strategies with all-virus-based expression of fluorophores, our design permits the visualization of multiple ensembles in a within-subject manner, which coalesces with previous studies monitoring and manipulating a single ensemble active at two discrete time points as well[28]. By intersecting these approaches with genetic sequencing strategies, these tools enable the tagging, manipulation, and molecular documentation of cells processing fear and reward, which opens the possibility of cataloguing topographical similarities and differences between the two in a brain-wide manner. For instance, we observed an upregulation of Alzheimer's related genes, including Ttr, APP, and APOE in cells processing negative memories, and neuroprotective-related genes in cells processing a positive memory including BDNF. APP is a key protein involved in AD, while BDNF has been shown to promote synapto- and dendritogenesis, fear extinction[27], and is decreased in a subset of patients with AD. Both provide future putative therapeutic targets for modulation in instances where these genes are dysfunctional.

Finally, while the physiological basis by which terminals can switch or reset their capacity to drive valence-specific behaviors remains unclear, future studies may consider candidate mechanisms including homeostatic plasticity, dendritic growth and retraction, and counter-conditioning-

facilitated changes along the axon-dendrite interface between vCA1 and the BLA or NAcc[25, 26]. In line with this speculation, previous studies have demonstrated that the dorsal hippocampus contains defined sets of functionally plastic cell bodies sufficient to drive fear or reward, while the BLA contains fixed populations that are sufficient to drive each behavior contingent on the anatomical location stimulated along the anterior-posterior axis as well as on their projection-specific sites.[7,8,25-27] Subsequent research can be aimed at utilizing our dual-memory tagging approach to genetically and physiologically map out which cell-types and circuits show such hardwired or experience-dependent responses to emotional memories as well.

Together, we propose that, in addition to processing spatio-temporal units of information, the hippocampus contains discrete sets of cells processing fear and reward that relay content-specific and behaviorally-relevant information to downstream areas in a molecularly-defined and projection-specific manner, thus collectively providing a multi-synaptic biological substrate for multiple memory engrams.

ONLINE METHODS

Subjects. Fos^{CreER} (Jax stock: #021882) and Wildtype male C57BL/6 mice (2-3 months of age; Charles River Labs) were housed in groups of 5 mice per cage. The animal vivarium was maintained on a 12:12-hour light cycle (lights on at 0700). Mice were placed on a diet containing 40 mg/kg doxycycline (Dox) for a minimum of 48 hours prior to surgery with access to food (doxycycline diet) and water *ad libitum*. Mice were given a minimum of ten days after surgery to recover. Dox-containing diet was replaced with standard mouse chow (*ad libitum*) 48 hours prior to behavioral tagging to open a time window of activity-dependent labeling[1,2]. All subjects were treated in accordance with protocol 17-008 approved by the Institutional Animal Care and Use Committee at Boston University.

Stereotaxic Surgery and Optic Implant. Stereotaxic injections and optical fiber implants follow methods previously reported.[1,2] All surgeries were performed under stereotaxic guidance and subsequent coordinates are given relative to bregma (in mm) dorsal ventral injections were calculated and zeroed out relative to the skull. Mice were placed into a stereotaxic frame (Kopf Instruments, Tujunga, CA, USA) and anesthetized with 3% isoflurane during induction and lowered to 1-2% to maintain anesthesia (oxygen L/min) throughout the surgery. Ophthalmic ointment was applied to both eyes to prevent corneal desiccation. Hair was removed with a hair removal cream and the surgical site was cleaned three times with ethanol and betadine. Following this, an incision was made to expose the skull. Bilateral craniotomies involved drilling windows through the skull above the injection sites using a 0.5 mm diameter drill bit. Coordinates were -3.16 anteroposterior (AP), ±3.1 mediolateral (ML), and -4.6 dorsoventral (DV) for vCA1; -1.8 AP, ± 3.1 ML, and -4.7 DV for the BLA; -2.0 AP, ±1.3 ML, and -2.0 DV for the DG; 1.25 AP, ± 1.0 ML, and -4.7 DV for the NAcc; 1.70 AP, ± 0.35 ML, and -2.8 DV for the PFC. All mice were

injected with a volume of 300nl of cocktail per site at a control rate of 100 µl min^{-1} using a mineral oil-filled 33-gage beveled needle attached to a 10 µl Hamilton microsyringe (701LT; Hamilton) in a microsyringe pump (UMP3; WPI). The needle remained at the target site for five minutes post-injection before removal. For all targets, bilateral optic fibers were placed 0.5 DV above the injection site. Jewelry screws secured to the skull acted as anchors. Layers of adhesive cement (C&B Metabond) followed by dental cement (A-M Systems) were spread over the surgical site. Mice received 0.1 mL of 0.3 mg/ml buprenorphine (intraperitoneally) following surgery and were placed on a heating pad during surgery and recovery. Histological assessment verified viral targeting and fiber placements. Data from off-target injections were not included in analyses.

Activity-dependent viral constructs. pAAV9-cFos-tTA, pAAV9-TRE-eYFP and pAAV9-TRE-mCherry were constructed as previously described (Ramirez et al., 2015). AAV9-c-Fos-tTA was combined with AAV9-TRE-eYFP or AAV9-TRE-ChR2-EYFP (UMass Vector core) prior to injection at a 1:1 ratio. This cocktail was further combined in a 1:1 ratio AAV9-CAG-Flex-DIO-TdTomato (UNC Vector Core).

Optogenetic Methods. Optic fiber implants were plugged into a patch cord connected to a 450nm laser diode controlled by automated software (Doric Lenses). Laser output was tested at the beginning of every experiment to ensure that at least 15 mW of power was delivered at the end of the patch cord (Doric lenses).

Behavior Tagging. When animals were off Dox, as previously reported[9-12], Dox diet was replaced with standard lab chow (*ad libitum*) 48-hours prior to behavioral tagging. Female exposure: One

female mouse (PD 30-40) was placed into a clean home cage with a clear cage top. The experimental male mouse was then placed into the chamber and allowed to interact freely for 2 hours. Fear exposure: Mice were placed into a conditioning chamber and received four 0.75mA (2s) foot shocks over an 8-minute training session. Following tagging, Dox was reintroduced to the diet and the male mice were returned to their home cage with access to Dox diet. For 4-OHT tagging, 40mg/kg was administered I.P. in Fos^{creER} mi 30 minutes following behavior and were left undisturbed for 72 hours. Mice were injected with saline at least one to two days prior to tagging protocol.

Behavioral Assays. All behavior assays were conducted during the light cycle of the day (0700–1900). Mice were handled for 3–5 days, 5-10 minutes per day, before all behavioral experiments. The testing chamber consisted of a custom-built rectangular box with a fiber optic holder (38 x 23.5 x 42 cm). Red tape divided the chamber down the middle, creating two halves. Right and left sides for stimulation were randomized. Day 1 was used to assess baseline levels, during which the mouse was given 10 minutes to freely explore the arena. The day following the first engram tag, mice received light stimulation (15 ms pulses at 20-Hz) upon entry in the designated side of the chamber (counterbalanced across groups) over a 10-minute test period. Once the mouse entered the stimulated side, a TTL signal from the EthoVision software via a Noldus USB-IO Box triggered a stimulus generator (STG-4008, Multi-channel Systems). 6A video camera (Activeon CX LCD Action Camera) recorded each session and an experimenter blind to treatment conditions scored the amount of time on each side. Statistical analyses involved a one-way ANOVAs comparing group difference scores [time (in seconds) on stimulated side minus time on unstimulated side]. Diagrams were made with BioRender.

Optogenetic Induction Protocol. For optogenetic fear induction, subjects were placed in a shock chamber with light stimulation (20 Hz, 15ms) for 500 second. Foot shocks (0.75 mA, 2s duration) were administered at the 198s, 278s, 358s, and 438s time points. During optogenetic reward induction, in a different room from the initial fear tag, clean home cages were used. Light stimulation (20Hz, 15ms) was applied to the male mouse for 10 minutes while exploring a female mouse.

Immunohistochemistry. Immunohistochemistry follows protocols previously reported[15, 16, 18]. Mice were overdosed with 3% isoflurane and perfused transcardially with cold (4° C) phosphate-buffered saline (PBS) followed by 4% paraformaldehyde (PFA) in PBS. Brains were extracted and stored overnight in PFA at 4°C. Fifty µm coronal sections were collected in serial order using a vibratome and collected in cold PBS. Sections were blocked for 1 hour at room temperature in PBST and 5% normal goat serum (NGS) on a shaker. Sections were transferred to wells containing primary antibodies (1:1000 guinea anti-c-Fos [SySy]; 1:1000 rabbit anti-RFP [Rockland]; 1:5000 chicken anti-GFP [Invitrogen]) and allowed to incubate on a shaker overnight at room temperature or 3 days at 4 degrees C. Sections were then washed in PBST for 10-min (x3), followed by 2-hour incubation with secondary antibody (1:200 Alexa 555 anti-rabbit [Invitrogen]; 1:200 Alexa anti-guinea 647 [Invitrogen]; 1:200 Alexa 488 anti-chicken [Invitrogen]). Following three additional 10-min washes in PBST, sections were mounted onto micro slides (VWR International, LLC). Vectashield Hart Set Mounting Medium with DAPI (Vector Laboratories, Inc) was applied, slides were cover slipped, and allowed to dry overnight.

Cell Quantification. Only animals that had accurate bilateral injections were selected for quantification. Fluorescent images were acquired using a confocal microscope (Zeiss LSM800,

Germany) at the 10X objective. All animals were sacrificed 90 minutes post-assay or optical stimulation for immunohistochemical analyses. The number of *c-Fos*-immunoreactive neurons in the BLA, PFC, and NAcc were counted to measure the number of active cells in the respective area of terminal stimulation and in the vCA1 the number of eYFP- or *c-Fos*-immunoreactive neurons were counted to measure the number of active cells during defined behavioral tasks in 3–5 coronal slices (spaced 50 um from each other) per mouse of which the means were taken. The number of eYFP-positive, TdTomato-positive, and *c-Fos*-positive, and DAPI-positive cells in a set region of interest (ROI) were quantified manually with ImageJ (https://imagej.nih.gov/ij/). The size of the ROI was standardized across brains, animals, experiments,and groups. Counters were blinded to experimental and control groups. To calculate the percentage of overlapping cells we counted the number of eYFP-positive cells and divided by the total number of DAPI-positive cells.

Generation of single cell suspension from mouse hippocampal tissue. Five-week old male mice labeled with ChR2-YFP transgene[1] after conditioning are euthanized by isoflurane. Mouse brains were rapidly extracted, and the hippocampal regions were isolated by microdissection. Eight mice were pooled by each experimental condition. Single cell suspension was prepared according to the guideline of Adult Brain Dissociation Kit (Miltenyi Botec, Cat No: 13-107-677). Briefly, the hippocampal samples were incubated with digestion enzymes in the C Tube placed on the gentleMACS Octo Dissociator with Heaters with gentleMACS Program: 37C_ABDK_01. After termination of the program, the samples were applied through a MACS SmartStrainer (70 μm). Then a debris removal step and a red blood cell removal steps were applied to obtain single cell suspension.

Isolation of YFP-positive single cell by FACS. The single cell suspension was subject to a BD FACSAria cell sorter according to the manufacturer's protocol to isolate YFP-single cell population.

Preparation of RNA-seq library. The RNA of FACS isolated YFP-positive cells was extracted by using Trizol (Life Technologies) followed by Direct-zol kit (Zymo Research) according to manufacturer's instructions. Then the RNA-seq library was prepared using SMART-Seq® v4 Ultra® Low Input RNA Kit (TaKaRa).

Analysis of RNA-seq data. The resulting 40 bp single-end reads from Illumina had good quality by checking with FastQC (http://www.bioinformatics.babraham.ac.uk/projects/fastqc/). Reads were mapped to MM10 using STAR[29], which was indexed with Ensembl GRCm38.91 Gene Annotation. The read counts were obtained using featureCounts[30] function from Subread package with strandness option as –r 0. Reads were normalized with DESeq2. The biological replicates in the neuron samples processed at different time periods, was corrected with remove BatchEffect from limma. Raw data along with gene expression levels were deposited to NCBI Gene Expression Omnibus GSE.

Sampling strategy. Subjects were randomly assigned to groups. No statistical methods were used to determine sample size; the number of subjects per group were based on those in previously published studies and are reported in figure captions.

Image Integrity. Acquired image files (.czi) were opened in ImageJ. Processing of images in Figure 1 involved maximizing intensity, removing outlier noise, and adjusting contrast of images.

Data Analysis. Data were analyzed using Prism (GraphPad Software, La Jolla, CA) and Statistica 13 data analysis software (TIBCO Software, Inc., Palo Alto, CA). Data were analyzed using paired t-tests (two factors), unpaired t-tests, one-way or two-way ANOVAs with repeated measures ANOVAs (more than two factors), where appropriate. Post-hoc analyses(Tukey's multiple comparisons test) were used to characterize treatment and interaction effects, when statistically significant alpha set at $p < 0.05$, two-tailed). Statistical analyses are reported in figure captions.

Reproducibility. Behavioral experiments were replicated at least twice with two different experimenters. Sequencing data was replicated twice as well to confirm original findings. All behavioral and cell counters and scorers were blinded to experimental and control groups.

Slice electrophysiology recording. Coronal slices of ventral hippocampus were prepared from previously injected animals, 3-5 days post tagging experience. Animals were deeply anesthetized with isoflurane anesthesia, decapitated and the brains were removed. Brain slices were prepared in oxygen perfused sucrose-substitute artificial cerebrospinal fluid (ACSF). Solution contained: 185 mM NaCl, 2.5 mM KCl, 1.25 mM NaH_2PO_4, mM $MgCl_2$, 25 mM $NaHCO_3$, 12.5 mM glucose, and 0.5 mM $CaCl_2$. 400 µm slices were cut via Leica VT 1200 (Leica Microsystems) and incubated in 30°C ACSF consisting of 125 mM NaCl, 25 mM $NaHCO_3$, 25 mM D-glucose, 2 mM KCl, 2 mM $CaCl_2$, 1.25 mM NaH_2PO_4, and 1 mM $MgCl_2$, for 20 minutes and then cooled to room-temperature. Two-photon imaging system (Thorlabs Inc.) was used to distinguish positive and negative cells. Imaging system is equipped with a mode-locked Ti:Sapphire laser (Chameleon Ultra II; Coherent) which was set to wavelengths between 920 nm to 950 nm in order to excite Alexa Fluor 488 and 568, tdTomato and EYFP fluorophores using a 20x , NA 1.0 objective lens (Olympus). In order to ensure differences between the two populations is not attributable to the

type of virus used for tagging the neurons, two groups of animals were prepared. In one group positive memories tagged with tdTomato and negative ones with EYFP and in the other one vice versa. Patch-clamp electrodes with 0.6–1 μm tips were pulled via horizontal puller (Sutter Instruments), and pipette resistance was recorded between 4 and 6 MΩ. Pipettes were filled with intracellular fluid containing: 120 mM K-gluconate, 20 mM KCl, 10 mM HEPES, 7 mM diTrisPhCr, 4 mM Na_2ATP, 2 mM $MgCl_2$, 0.3 mM Tris-GTP, and 0.2 mM EGTA; buffered to pH 7.3 with KOH. 0.15% weight/volume of Alexa Fluor (Thermo Fisher Scientific) 488 hydrazide (for recording from tdTomato cells) or 567 (for recording from EYFP cells) were added to visualize the recording pipette under the imaging system. Prior to breaking into the cells, pipette capacitance neutralization and bridge balance compensation were performed . Data was acquired using Multiclamp 700B (Molecular Devices) and a Digidata 1550 (Molecular Devices) with sampling rate of 10kHz.

Electrophysiology data analysis. Brain slice electrophysiology data analysis was performed in python with custom written scripts using pyABF package (http://swharden.com/pyabf/). For spike shape analysis , spike onsets were identified using their first derivative, corresponding voltage was called spike onset. Spike half-width indicates the time between the two halves of peak voltage. For dynamic analysis of spiking properties stepwise current injections were performed. Firing threshold is the voltage at which a neuron fires at least a single spike, and firing onset is the corresponding current. FI gain was calculated as change in the firing frequency from the lowest to the highest frequency of firing divided by current injected. Adaptation ratio was obtained by dividing the mean inter spike intervals (ISIs) during the last 200 ms of spiking by the mean ISIs during the first 200 ms of spiking. Comparison between positive and negative memory cells were done both within a single slice, within an animal as well as across animals to control for potential

differences between animals or slices. Since the results in all three situations were similar, the pooled data. For comparison of different groups d'Agostino-Pearson K2 test was used to determine normality of data. Based on the normality results, either independent t-test (normal distribution) or Mann-Whitney-Wilcoxon test two-sided with Bonferroni correction were used.

Figure Descriptions

Figure 1 | Hippocampus cells processing positive or negative memory engrams are preferentially reactivated by their respective valences

a, Fos-CreERT2 were injected with a virus cocktail of AAV-Flex-DIO-TdTomato, AAV9-c-Fos-tTA and AAV9-TRE-EYFP into vCA1for Experience 1 and Experience 2 respectively. Experience 3 is reflected by endogenous cFos, 90 minutes after behavior. **b**, Schematic of groups for visualizing triple memory overlaps (n=4-6 per group). **c-d**, Representative images of triple memory overlaps in vCA1 with a 20x zoom in showing the different representative overlaps. **e**, The number of tagged neurons in vCA1 are similar between shock (hereafter to referred to as the "Negative Group") and female exposure (hereafter referred to as the Positive Group) across all three experiences, EYFP (t_{46}=1.24, NS[Not Significant]), TdTomato (t_{46}=0.45, NS), cfos (t_{46}=1.85, NS). **f-i**, Percentage overlap for respective behavioral tags **f**, EYFP + Tdtomato, (F (3, 12) = 170.0, P<0.0001); **g**, EYFP + cfos, (t_{12}=1.300); **h**, TdTomato + cFos, (F (3, 12) = 20.77, P<0.0001); **i**, T overlap counts of EYFP + TdTomato + cfos (F (3, 12) = 10.55, P=0.0011) **j-m**, Scaled Venn Diagrams showing the number of green, red, and purple neurons and their respective overlaps in vCA1 in the 4 experimental groups

Figure 2 | Hippocampus cell bodies processing positive or negative memory engrams show similar electrophysiological properties

a, Fos-CreERT2 were injected with a virus cocktail of AAV-Flex-DIO-TdTomato, AAV9-c-Fos-tTA and AAV9-TRE-EYFP to tag either negative or positive experiences within the same animal for slice electrophysiology. **b**, Representative image of cells processing a negative (red) or positive (green) experience. **c**, Representative voltage responses to -100, -50, 0, 50 and 150 pA of step current injection in negative (red) and positive (green) engram cells. **d**, Average firing frequency

corresponding to current injection (FI curve) (negative engrams: n=10, positive engrams: n=17) . Error bars correspond to standard error and no point of the curve was significantly different between the two populations. **e-g**, Suprathreshold characterization current-voltage responses of tagged hippocampal neurons. **e**, FI gain is the slope of the linear part of the FI curve shown in B, calculated as the change in firing frequency from the minimum firing to maximum firing divided by the injected current. **h-i**, Voltage and current step at which the neuron had at least one spike. **h**, Adaptation ratio is calculated as the mean inter spike interval (ISI) during the last 200 ms of spiking divided the mean ISI during the first 200 ms of spiking during a current step corresponding to 20 Hz firing rate. **i**, Input resistance for each neuron, calculated by averaging 25 trials for change in voltage divided by 25 pA injected while holding the cell at -70 mV. **j-l**, Analysis of spike shape of cells tagged by negative or positive experiences. **j**, Spike traces from all the negative and positive cells (Bold trace corresponds to average trace shape) **k**, Spike half width calculated as the time duration between two midpoints of the spikes. **l**, Deflection point of spike as identified by its first derivative. P-values were calculated based on independent t-test or Mann-Whitney test depending on normality of data.

Figure 3 | Molecular landscapes of positive and negative hippocampus engram cells

a, Experimental scheme to label, isolate, and analyze the two groups of engram neurons. **b-d.** FACS isolation of GFP-positive nuclei from the hippocampi of mice labeled by AAV9-cFos-tTA + AAV9-TRE-ChR2-EYFP virus from their respective groups **e**, Percentage of GFP-positive nuclei from each group. **f**, Volcano plot in the upper panel shows the gene expressions of neurons active during negative or positive experiences that were subsequently isolated from the hippocampus. Heat map in the lower panel shows the top 30 differentially expressed genes identified between negative and mock cells. **g**, Gene Enrichment Set Analysis of the differentially

expressed genes between negative, positive, and mock samples. Gene Ontology (GO) enrichment analysis (Cellular Component) of all genes between negative and positive samples. Gene Ratio is the ratio of the number of genes enriched in the GO term to the total genes numbers in the GO term, Count is the number of enriched genes, and p.adjust is the Benjamini-Hochberg (BH) corrected p value indicating the significance of the GO term enrichment. The size of the dot represents the gene count and the color of the dot indicates the adjusted p value.

Figure 4 | Hippocampal outputs are sufficient to drive avoidance and preference in a projection-specific and functionally reversible manner

a, Mice were injected with a virus cocktail of AAV9-c-Fos-tTA and AAV9-TRE-EYFP into vCA1 and optic fibers were placed bilaterally over the BLA, Nacc, or the PFC, in separate groups. The mice were then tagged with either a negative or positive experience and subjected to real time opto-place avoidance and preference. **b**, Representative images of ChR2-EYFP labeling cell bodies in vCA1 and its respective terminals in the BLA, NAcc, and PFC. **c**, Fear to reward protocol in which the subjects received stimulation of BLA, NAcc, or PFC terminals originating from vCA1. **d**, Percent preference for the stimulation side at baseline, pre-induction, and post-induction (n = 7 subjects for EYFP controls, n = 8 subjects for BLA, n = 7 for NAcc, and n = 7 for PFC, **P = 0.0018, ***P = 0.0006, repeated measures one-way ANOVA followed by Tukey's multiple comparison test). **e**, Reward to Fear protocol in which the subjects received stimulation of BLA, NAcc, or PFC terminals originating from vCA1. **f**, Percent preference for the stimulation side at baseline, pre-induction, and post-induction (n = 7 subjects for EYFP, n = 8 subjects for BLA, n = 7 for NAcc, and n = 7 for PFC, **P = 0.0032, ****P < 0.0001, repeated measures one-way ANOVA followed by Tukey's multiple comparison test).

Acknowledgements.

We thank Dr. Joshua Sanes and his lab at the Center for Brain Science, Harvard University, for providing laboratory space within which the initial experiments were conducted, the Center for Brain Science Neuroengineering core for providing technical support, and the Society of Fellows at Harvard University for their support. This work was supported by an NIH Early Independence Award (DP5 OD023106-01), an NIH Transformative R01 Award, a Young Investigator Grant from the Brain and Behavior Research Foundation, a Ludwig Family Foundation grant, the McKnight Foundation Memory and Cognitive Disorders award, and the Center for Systems Neuroscience and Neurophotonics Center at Boston University.

Author Contributions

M.S., O.M., and E.R. conducted and analyzied histological and optogenetic experiments, B.Y. and X.S.L. performed RNA sequencing and corresponding analyses, B.R. and F.R.F. conducted in vitro physiological experiments and analyses, M.S., O.M., S.L.G., and S.R. designed the project, and M.S. and S.R. wrote the manuscript. All authors edited and commented on the manuscript.

Declaration of Interests

The authors declare no competing interests.

References

1. Josselyn, S.A. & Tonegawa, S. Memory engrams: Recalling the past and imagining the future. *Science* **367**(6473) (2020)
2. Josselyn, S., Köhler, S. & Frankland, P. Finding the engram. *Nat Rev Neurosci* **16,** 521–534 (2015)
3. Cai, D. J., et al. A shared neural ensemble links distinct contextual memories encoded close in time, *Nature* **000**, 1-4 (2016).
4. M. S. Fanselow, M. S. & Dong, H.W., Neuron 65, 7–19 (2010).
5. Gaurgier J. L. & Tank, D. W. A dedication population for reward coding in the hippocampus, *Neuron* **99**, 179-193 (2018).
6. Xu, C. et al. Distinct hippocampal pathways mediate dissociable roles of context in memory retrieval, *Cell* **167**, 1-2 (2016).
7. Ciocchi, S., Passecker, J., Malagon-Vina, H., Mikus, N., & Klausberger, T. Selective information routing by ventral hippocampal CA1 projection neurons, *Science* 348, 560-563 (2015).
8. Padilla-Coreano, N. et al. Direct Ventral Hippocampal-Prefrontal Input is Required for Anxiety-Related Neural Activity and Behavior, *Neuron* **89**, 857-866 (2016).
9. Kim, J., Pignatelli, M., Xu, S., Itohara, S. & Tonegawa, S. Antagonistic negative and positive neurons of the basolateral amygdala. *Nat. Neurosci.* **19**, 1636–1646 (2016).
10. Liu, X. et al. Optogenetic stimulation of a hippocampal engram activates fear memory recall. *Nature* **484**, 381–385 (2012).
11. Ramirez, S. et al. Creating a false memory in the hippocampus. *Science* **341**, 387–391 (2013).

12. Redondo, R. L. et al. Bidirectional switch of the valence associated with a hippocampal contextual memory engram. *Nature* **513**, 426–430 (2014).

13. Ryan, T. J., Roy, D. S., Pignatelli, M., Arons, A. & Tonegawa, S. Engram cells retain memory under retrograde amnesia. *Science* **348**, 1007–1013 (2015).

14. Gore, F. et al. Neural representations of unconditioned stimuli inn basolateral amygdala mediate innate and learned responses. *Cell***162,** 134-145 (2015).

15. Rashid, A. J. et al. Competition between engrams influences fear memory formation and recall, *Science* **353**, 383-38 (2017).

16. Yokose, J. et al. Overlapping memory trace indispensable for linking, but not recalling, individual memories, *Science* **355**, 398-403 (2017).

17. DeNardo, L. A. et al. Temporal evolution of cortical ensembles promoting remote memory retrieval. *Nature Neuroscience* ***22*(3)**, 460–469. (2019).

18. Ramirez, S., Liu, X., MacDonald, C. *et al.* Activating positive memory engrams suppresses depression-like behaviour. *Nature* **522,** 335–339 (2015).

19. Chen, B. K., Murawski, N. J., et al Artificially enhancing and suppressing hippocampus-mediated memories. *Current Biology*, **29(11)**, 1885-1894.e4 (2019)

20. Rodriguez, E. et al. Identifying Parabrachial neurons selectively regulating satiety for highly palatable food in mice. *Eneuro* **6(6)**, ENEURo.0252-19 .(2019)

21. Peters, J., Dieppa-Perea,L. M., Melendez, L. M., & Quirk, G. J. Induction of fear extinction with hippocampal-infralimbic BDNF, *Science* **328**, 1288-1290 (2010).

22. Gan, L., Cookson, M.R., Petrucelli, L. *et al.* Converging pathways in neurodegeneration, from genetics to mechanisms. *Nat Neurosci* **21,** 1300–1309 (2018).

23. Warden, M.R. et al. A prefrontal cortex-brainstem neuronal projection that controls response to behavioural challenge, *Nature* **428**428-432 (2012).

24. Beyeler, A. et al. Divergent Routing of Positive and Negative Information from the Amygdala during Memory Retrieval, *Neuron* **90,**348-361 (2016).

25. Namburi, P. et al. A circuit mechanism for differentiating positive and negative associations, *Nature* **520**, 675-678 (2015).

26. Jimenez, J. C. et al. Anxiety cells in a hippocampal-hypothalamic circuit. *Neuron* **97**. 1-14 (2018).

27. Spellman, T., Rigotti, M., Ahmari, S. *et al.* Hippocampal–prefrontal input supports spatial encoding in working memory. *Nature* **522,** 309–314 (2015).

28. Xiu, J., Zhang, Q., Zhou, T. *et al.* Visualizing an emotional valence map in the limbic forebrain by TAI-FISH. *Nat Neurosci* **17,** 1552–1559 (2014).

29. Dobin, A, et al. STAR: ultrafast universal RNA-seq aligner, *Bioinformatics* **29**, 15-21 (2013).

30. Liao,Y., Smyth, G.K., & Shi, W. featureCounts: an efficient general purpose program for assigning sequence reads to genomic features, *Bioinformatics* **30**, 923-930 (2014).

Extended Data Figures

Extended Data Fig 1: Ventral CA1 cells active during positive or negative experiences recruit statistically distinct sets of cells. a, Representative images of cells tagged by a positive experience (green, EYFP) as measured by cFos-tTA-driven TRE-EYFP expression, and subsequently active during a negative experience (red, cFos), as measured by endogenous cFos. **b**, Overlap counts of cFos-positive and EYFP-positive cells (observed) compared to a statistically expected count. **c**, Representative overlaps between cells tagged by a negative experience (green, EYFP) and active during a subsequent negative experience (red, cFos); **d**, Same as in **b,** except both experiences are negative. **e-f**, Same as above, except both experiences are positive. (n = 5 mice, 3 slices per mouse averaged across each animal; ****P<0.0001, NS = Not significant, unpaired student's t-test).

Extended Data Fig. 2: Volcano plots for hippocampus cells processing positive and negative memory engrams

a, Principle component analysis of RNA-seq data of positive, negative, and mock samples. **b**, The volcano plot on the left shows the gene expression patterns of previously active neurons isolated from the hippocampi of mice that underwent fear conditioning (Negative), compared to hippocampal neurons from naive (mock) mice. The heat map in **b**, shows the top 20 or 30 differentially expressed genes identified between negative and mock groups. **c**, The volcano plot on the right shows a similar gene expression analysis but between hippocampal cells previously active during a positive experience compared to mock samples positive and mock groups

Extended Data Fig. 3: Hippocampus cells tagged during a positive or negative experience upregulate neuroprotective and neurodegenerative genes, respectively.

a, Gene Enrichment Set Analysis of neuroprotective genes between negative, positive, and mock samples. **b**, Gene Enrichment Set Analysis of neurodegenerative disease-related genes between negative, positive, and mock samples. Gene sets can be found in Table3 and Table4.

Extended Data Fig. 4: Negative vs mock cells GO analysis. a, biological process, **b**, cellular component, **c**, molecular function.

Extended Data Fig. 5: Positive vs mock GO analysis. a, biological process, **b**, cellular component **c**, molecular function.

Extended Data Fig. 6: Stimulation of vCA1 cell bodies does not drive preference or avoidance. a, Mice were injected with a virus cocktail of AAV9-c-Fos-tTA and AAV9-TRE-EYFP into vCA1 and optic fibers were placed above the injection site. The animals were then tagged with either shock (Negative Group) or female exposure (Positive Group) and tested for opto-place avoidance or preference. **b**, Negative and Positive experiences labeled a similar proportion of EYFP-positive vCA1 cells. (t_{24}=1.32) **c**, Fear to reward experimental protocol. (**d-f**) Animal's percent preference for the optically stimulated side, **d,** baseline, **e**, Pre-Induction, and **f**, Post-Induction (n = 6 subjects for EYFP and n = 6 subjects for ChR2-EYFP, $P > 0.05$ repeated measures one-way ANOVA followed by Tukey's multiple comparison test). **g**, Reward to fear experimental protocol. **h-j**, Animal's percent preference for the optically stimulated side, **h**,

baseline, **i**, Pre-Induction, and **j**, Post-Induction (n = 6 subjects for EYFP and n = 6 subjects for ChR2-EYFP, $P > 0.05$ repeated measures one-way ANOVA followed by Tukey's multiple comparison test, data presented from Post-Hoc Analysis).

Extended Data Fig. 7: Terminal-specific optogenetic stimulation of vCA1 outputs leads to increased cFos in target areas

a, d, g, Representative images of ChR2-EYFP in BLA, NAcc, and PFC terminals, respectively, and cFos expression after optical reactivation. **b, e, h**, Representative images of cFos without optogenetic reactivation of corresponding vCA1 terminals. **c, f, i**, Percent cFos/DAPI of BLA, NAcc, and PFC non- stim vs stim groups (**P =0.0014, ****P < 0.0001 unpaired student's t-test)

Extended Data Fig. 8: Terminal-specific optogenetic stimulation of vCA1 outputs did not affect distance travelled in all groups. Stimulation of vCA1 terminals over the **a**, BLA (n=8), **b**, NAc (n=10), or **c**, PFC (n=9), had no effect on the distance travelled between light on or off epochs and across pre-induction or post-induction timepoints.

Extended Data Fig. 9: Altering stimulation frequency or activating cells processing a neutral memory does not lead to changes in avoidance or preference. a, Behavioral schedule in which vCA1 terminals are tagged in a neutral homecage experience (depicted as a purple square during the off Dox period), followed by the induction protocol in which these outputs are activated concurrently during a positive experience in the **b**, BLA or **e**, NAcc. Mice were injected with a virus cocktail consisting of cFos-tTa + TRE-ChR2-EYFP. **c, f**, Percent preference for the stimulation side when optically activating vCA1 terminals over the BLA or NAcc at 20Hz during baseline, pre-induction, and post-induction tests. **d, g**, Percent preference for the stimulation side

when optically activating vCA1 terminals over the BLA or NAcc at 4hz during baseline, pre-induction, and post-induction tests. **h**, Same as in **a,** except vCA1 terminals are concurrently activated during a negative experience. **i, k**, Percent preference for the stimulation side at 20 Hz during baseline, pre-, and post-induction tests. **d, g**, Percent preference for the stimulation side at 4Hz during baseline, pre-induction, and post-induction (n = 6 subjects for all groups; NS = not significant; repeated measures one-way ANOVA followed by Tukey's multiple comparison test).

Figure 1

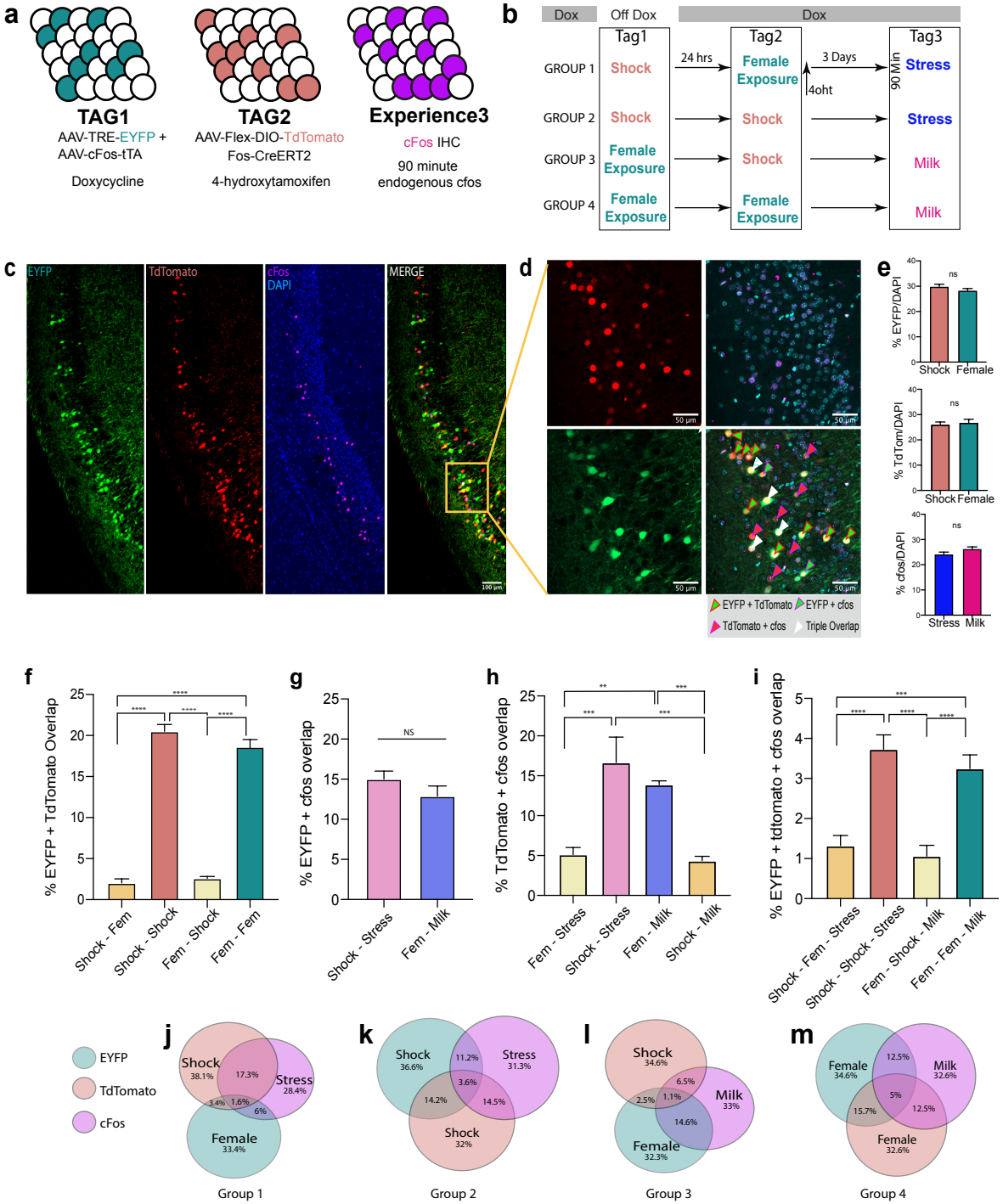
a
TAG1
AAV-TRE-EYFP +
AAV-cFos-tTA
Doxycycline
TAG2
AAV-Flex-DIO-TdTomato
Fos-CreERT2
4-hydroxytamoxifen
Experience3
cFos IHC
90 minute
endogenous cfos
b
Dox
Off Dox
Dox
Tag1
Tag2
Tag3
GROUP 1
Shock
24 hrs
Female Exposure
3 Days
4oht
90 Min
Stress
GROUP 2
Shock
Shock
Stress
GROUP 3
Female Exposure
Shock
Milk
GROUP 4
Female Exposure
Female Exposure
Milk
c
EYFP
TdTomato
cFos
DAPI
MERGE
d
EYFP + TdTomato
EYFP + cfos
TdTomato + cfos
Triple Overlap
e
% EYFP/DAPI
% TdTom/DAPI
% cfos/DAPI
ns
Shock
Female
Stress
Milk
f
% EYFP + TdTomato Overlap
Shock - Fem
Shock - Shock
Fem - Shock
Fem - Fem
g
% EYFP + cfos overlap
NS
Shock - Stress
Fem - Milk
h
% TdTomato + cfos overlap
Fem - Stress
Shock - Stress
Fem - Milk
Shock - Milk
i
% EYFP + tdtomato + cfos overlap
Shock - Fem - Stress
Shock - Shock - Stress
Fem - Shock - Milk
Fem - Fem - Milk
EYFP
TdTomato
cFos
j
Shock 38.1%
17.3%
Stress 28.4%
3.4%
1.6%
6%
Female 33.4%
Group 1
k
Shock 36.6%
11.2%
Stress 31.3%
3.6%
14.2%
14.5%
Shock 32%
Group 2
l
Shock 34.6%
6.5%
2.5%
1.1%
Milk 33%
14.6%
Female 32.3%
Group 3
m
Female 34.6%
12.5%
Milk 32.6%
5%
15.7%
12.5%
Female 32.6%
Group 4

Figure 2

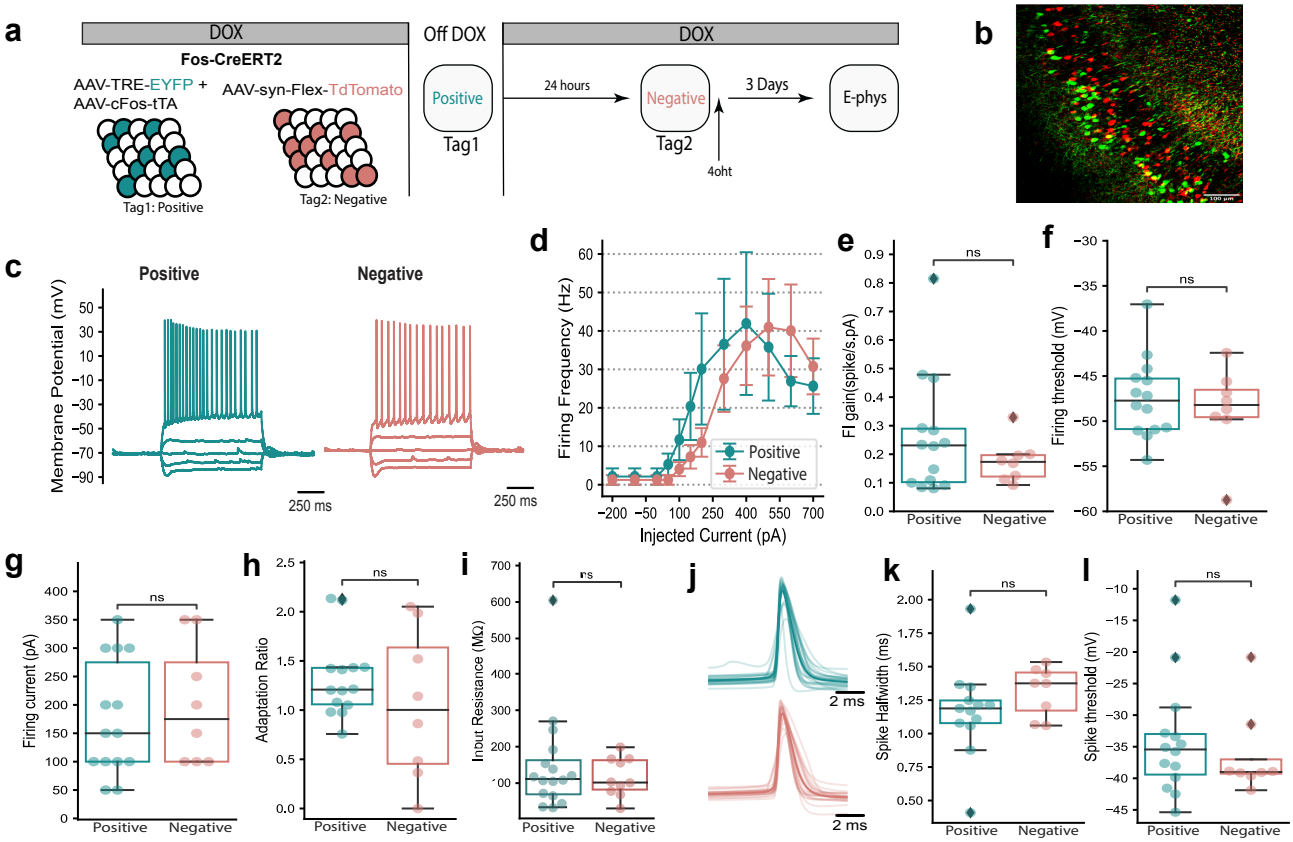
a
DOX
Fos-CreERT2
AAV-TRE-EYFP +
AAV-cFos-tTA
AAV-syn-Flex-TdTomato
Tag1: Positive
Tag2: Negative
Off DOX
DOX
Positive
Tag1
24 hours
Negative
Tag2
4oht
3 Days
E-phys
b
c
Positive
Negative
Membrane Potential (mV)
250 ms
250 ms
d
Firing Frequency (Hz)
Positive
Negative
Injected Current (pA)
e
ns
FI gain(spike/s.pA)
Positive
Negative
f
ns
Firing threshold (mV)
Positive
Negative
g
ns
Firing current (pA)
Positive
Negative
h
ns
Adaptation Ratio
Positive
Negative
i
ns
Inpout Resistance (MΩ)
Positive
Negative
j
2 ms
2 ms
k
ns
Spike Halfwidth (ms)
Positive
Negative
l
ns
Spike threshold (mV)
Positive
Negative

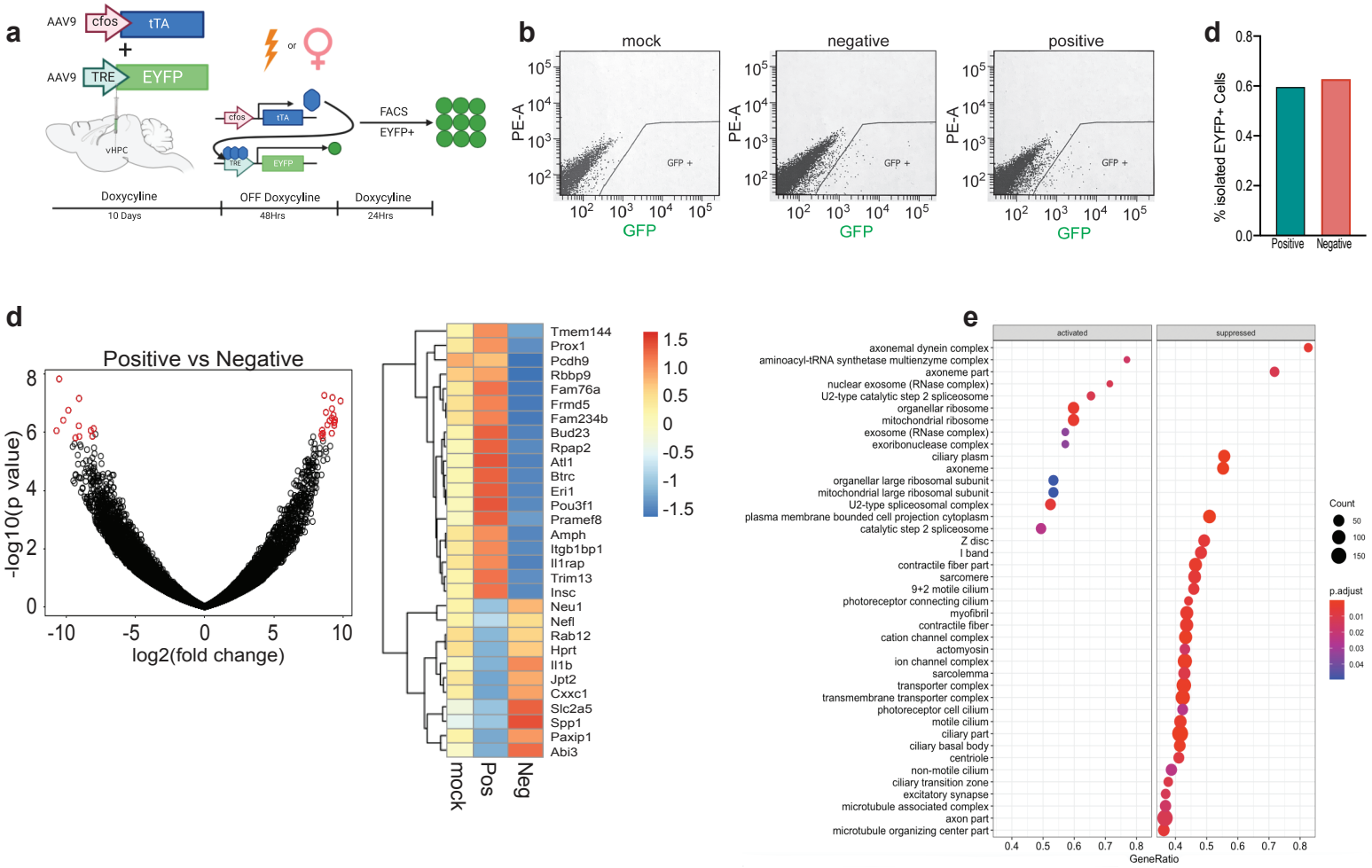
a
AAV9
cfos
tTA
+
AAV9
TRE
EYFP
vHPC
or
FACS
EYFP+
Doxycyline
10 Days
OFF Doxycyline
48Hrs
Doxycyline
24Hrs
b
mock
negative
positive
PE-A
GFP
GFP +
d
% isolated EYFP+ Cells
Positive
Negative
d
Positive vs Negative
-log10(p value)
log2(fold change)
Tmem144
Prox1
Pcdh9
Rbbp9
Fam76a
Frmd5
Fam234b
Bud23
Rpap2
Atl1
Btrc
Eri1
Pou3f1
Pramef8
Amph
Itgb1bp1
Il1rap
Trim13
Insc
Neu1
Nefl
Rab12
Hprt
Il1b
Jpt2
Cxxc1
Slc2a5
Spp1
Paxip1
Abi3
mock
Pos
Neg
e
activated
suppressed
axonemal dynein complex
aminoacyl-tRNA synthetase multienzyme complex
axoneme part
nuclear exosome (RNase complex)
U2-type catalytic step 2 spliceosome
organellar ribosome
mitochondrial ribosome
exosome (RNase complex)
exoribonuclease complex
ciliary plasm
axoneme
organellar large ribosomal subunit
mitochondrial large ribosomal subunit
U2-type spliceosomal complex
plasma membrane bounded cell projection cytoplasm
catalytic step 2 spliceosome
Z disc
I band
contractile fiber part
sarcomere
9+2 motile cilium
photoreceptor connecting cilium
myofibril
contractile fiber
cation channel complex
actomyosin
ion channel complex
sarcolemma
transporter complex
transmembrane transporter complex
photoreceptor cell cilium
motile cilium
ciliary part
ciliary basal body
centriole
non-motile cilium
ciliary transition zone
excitatory synapse
microtubule associated complex
axon part
microtubule organizing center part
GeneRatio
Count
p.adjust

Figure 4

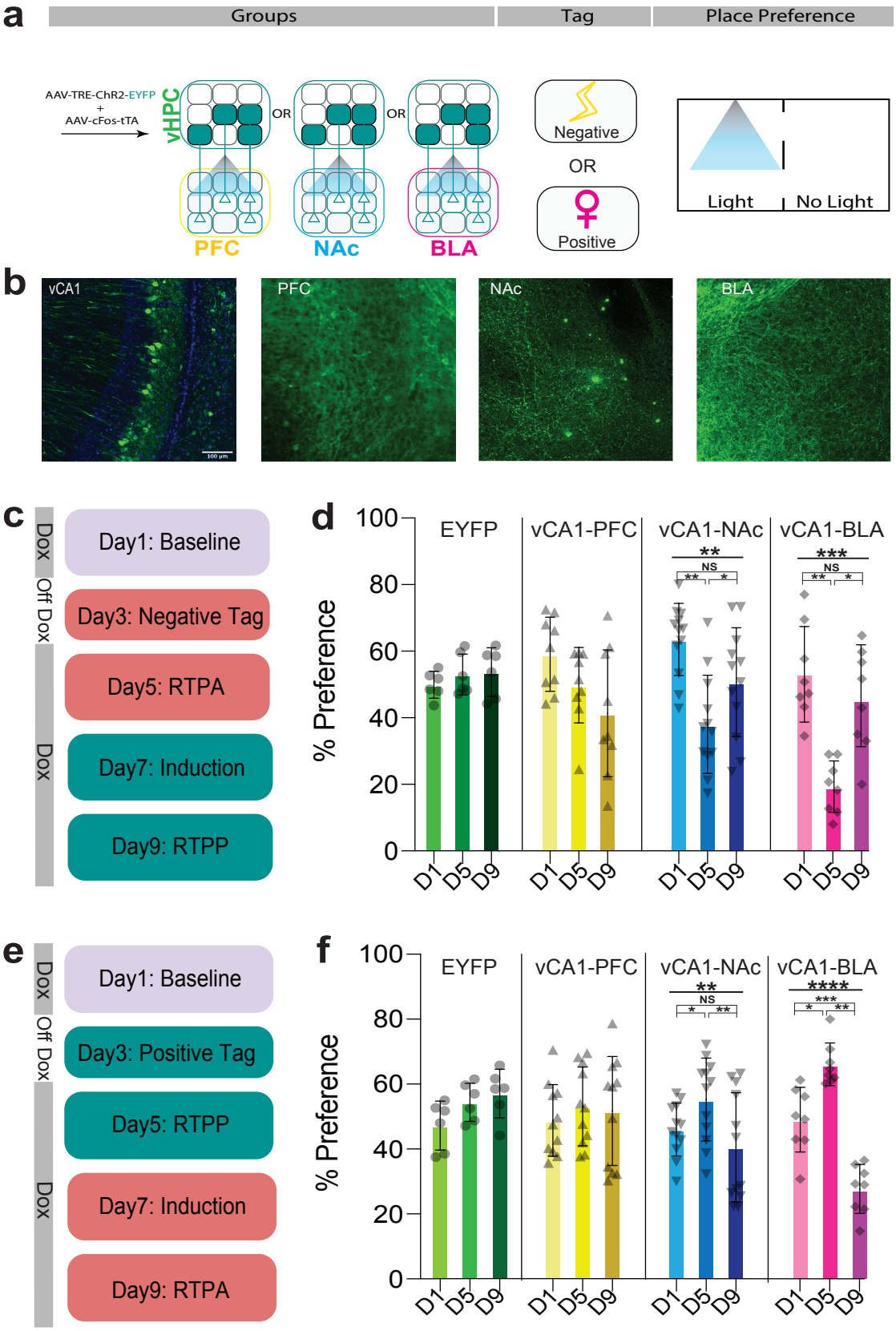
a
Groups
Tag
Place Preference
AAV-TRE-ChR2-EYFP
+
AAV-cFos-tTA
vHPC
OR
OR
PFC
NAc
BLA
Negative
OR
Positive
Light
No Light
b
vCA1
PFC
NAc
BLA
c
Dox
Off Dox
Dox
Day1: Baseline
Day3: Negative Tag
Day5: RTPA
Day7: Induction
Day9: RTPP
d
% Preference
EYFP
vCA1-PFC
vCA1-NAc
vCA1-BLA
D1
D5
D9
e
Dox
Off Dox
Dox
Day1: Baseline
Day3: Positive Tag
Day5: RTPP
Day7: Induction
Day9: RTPA
f
% Preference
EYFP
vCA1-PFC
vCA1-NAc
vCA1-BLA
D1
D5
D9

Extended Data Figure 1

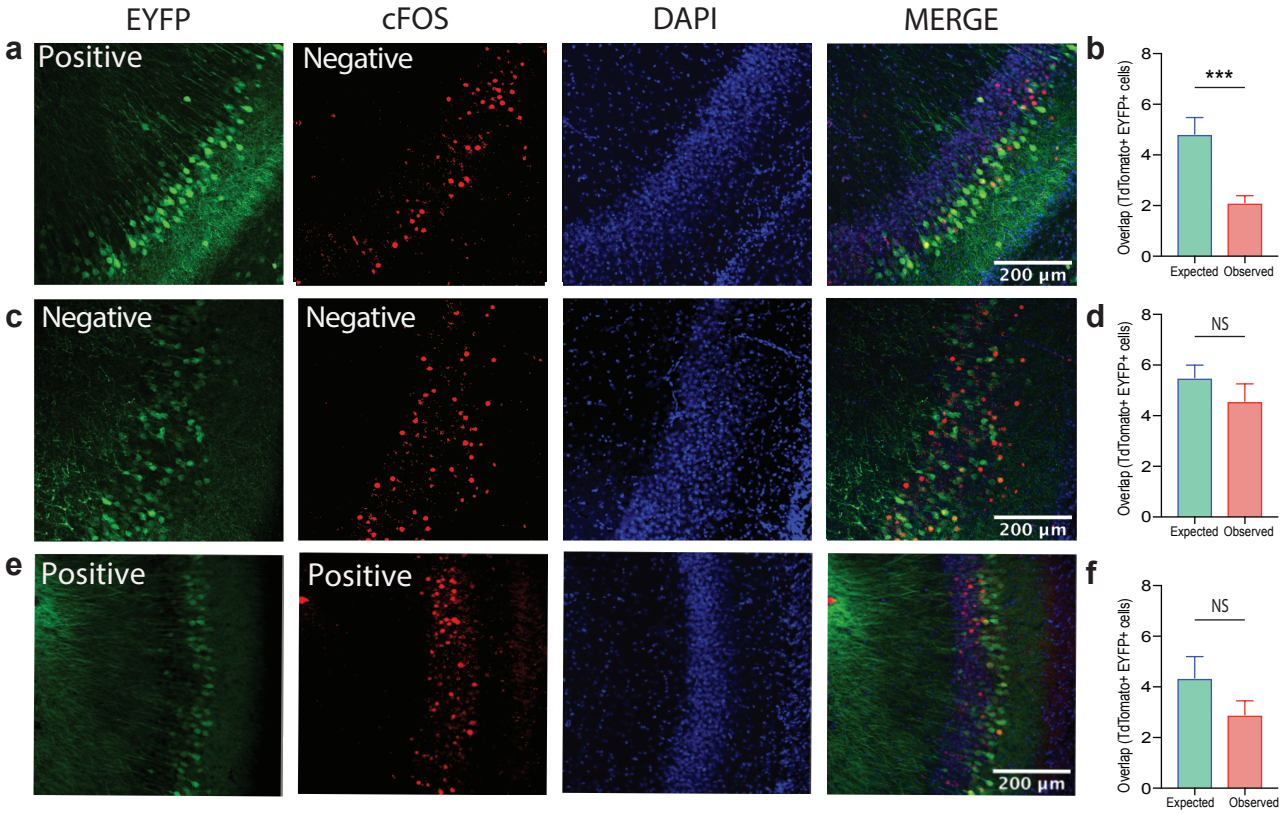

Extended Data Figure 2

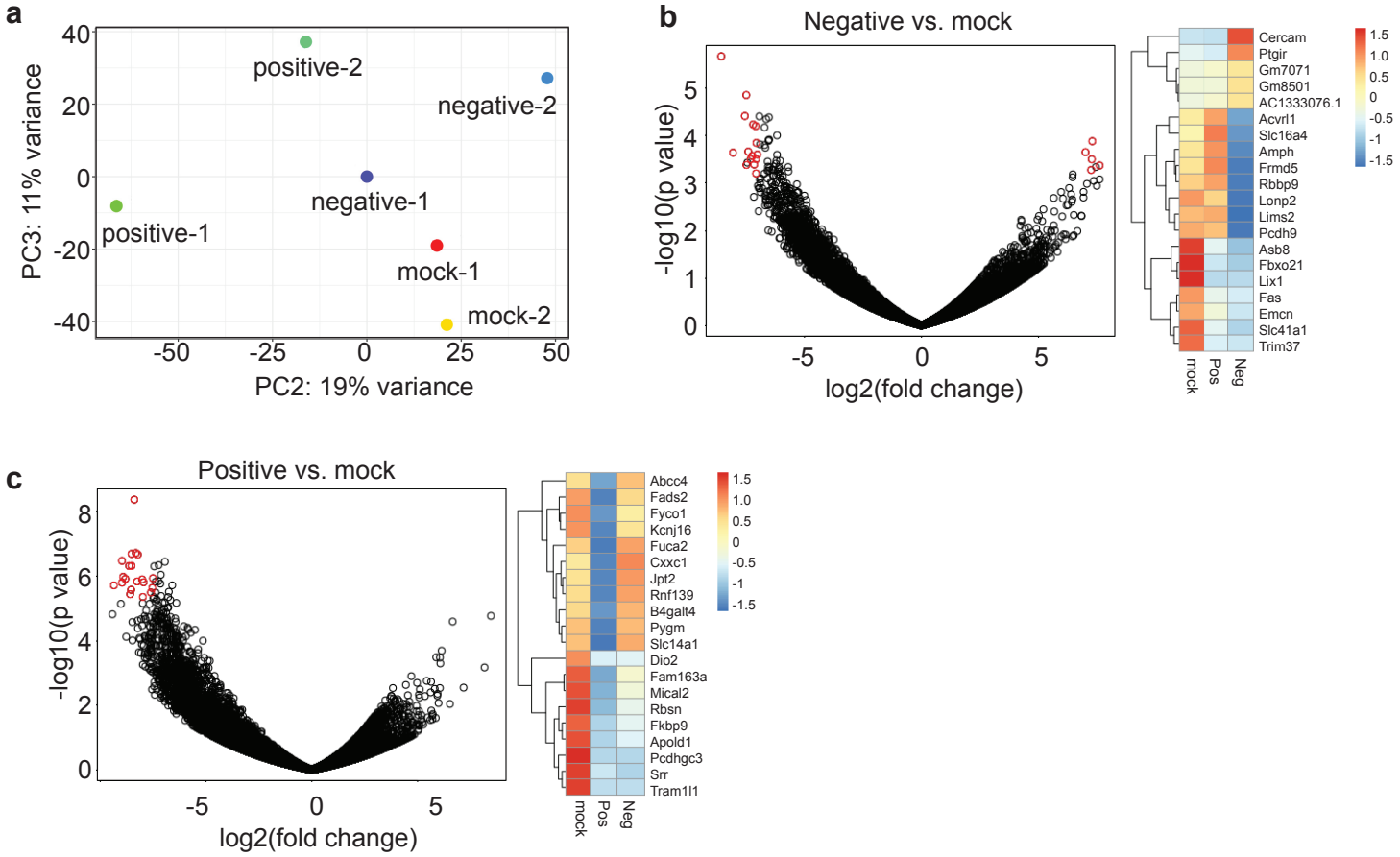

Extended Data Figure 3

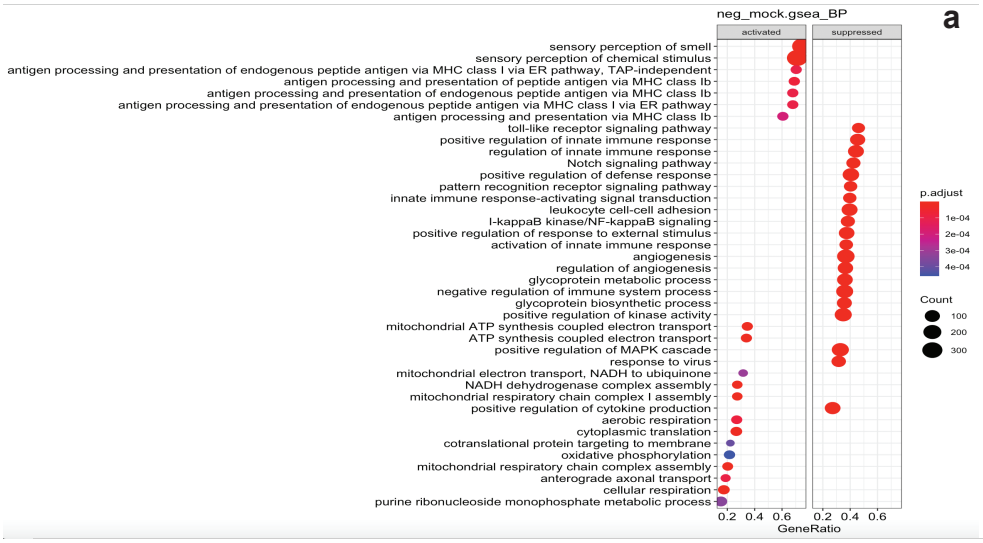

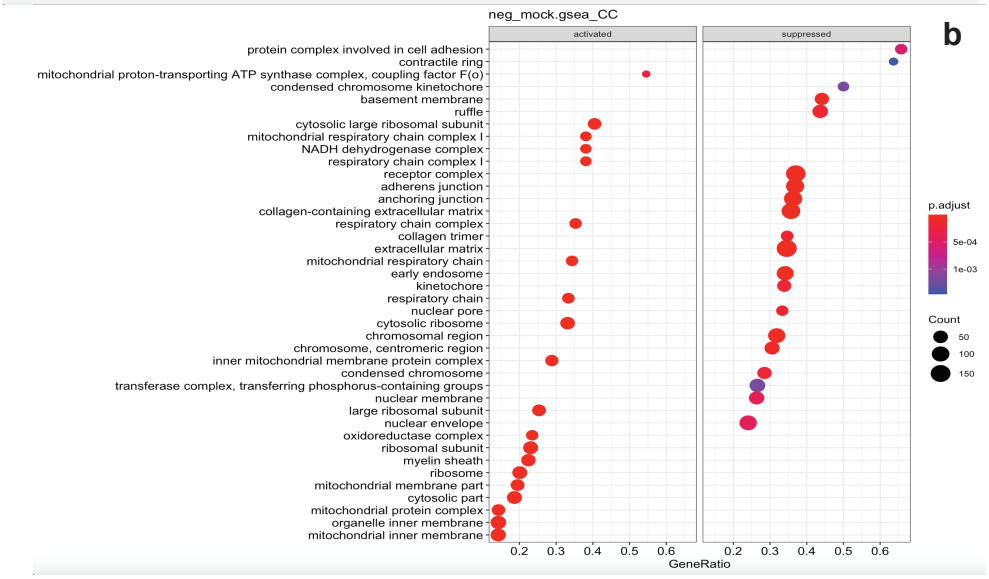

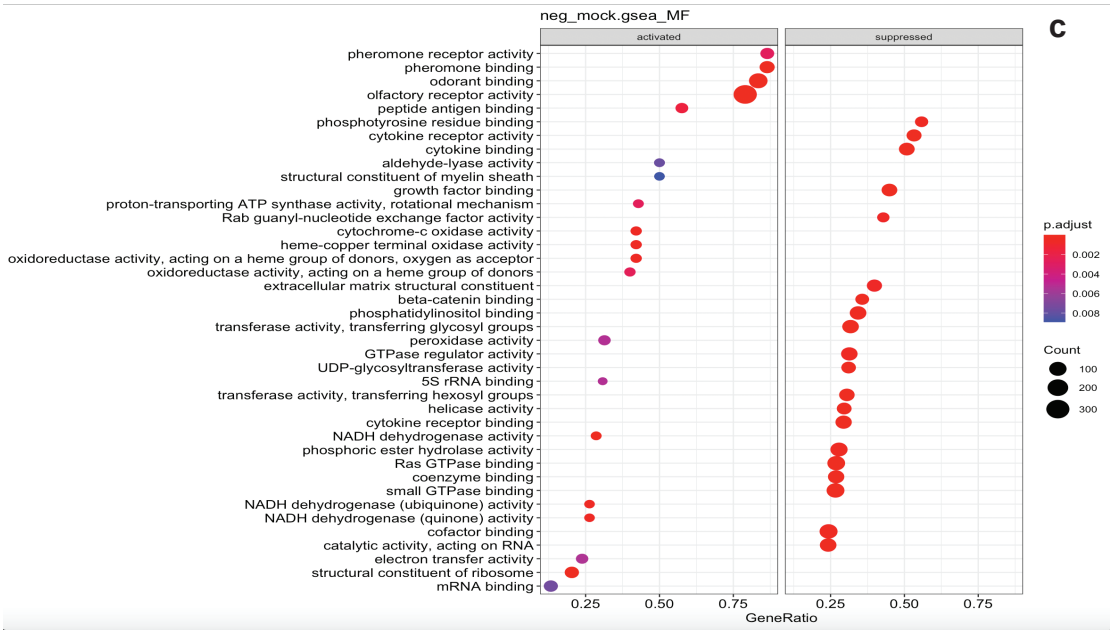

Extended Data Figure 4

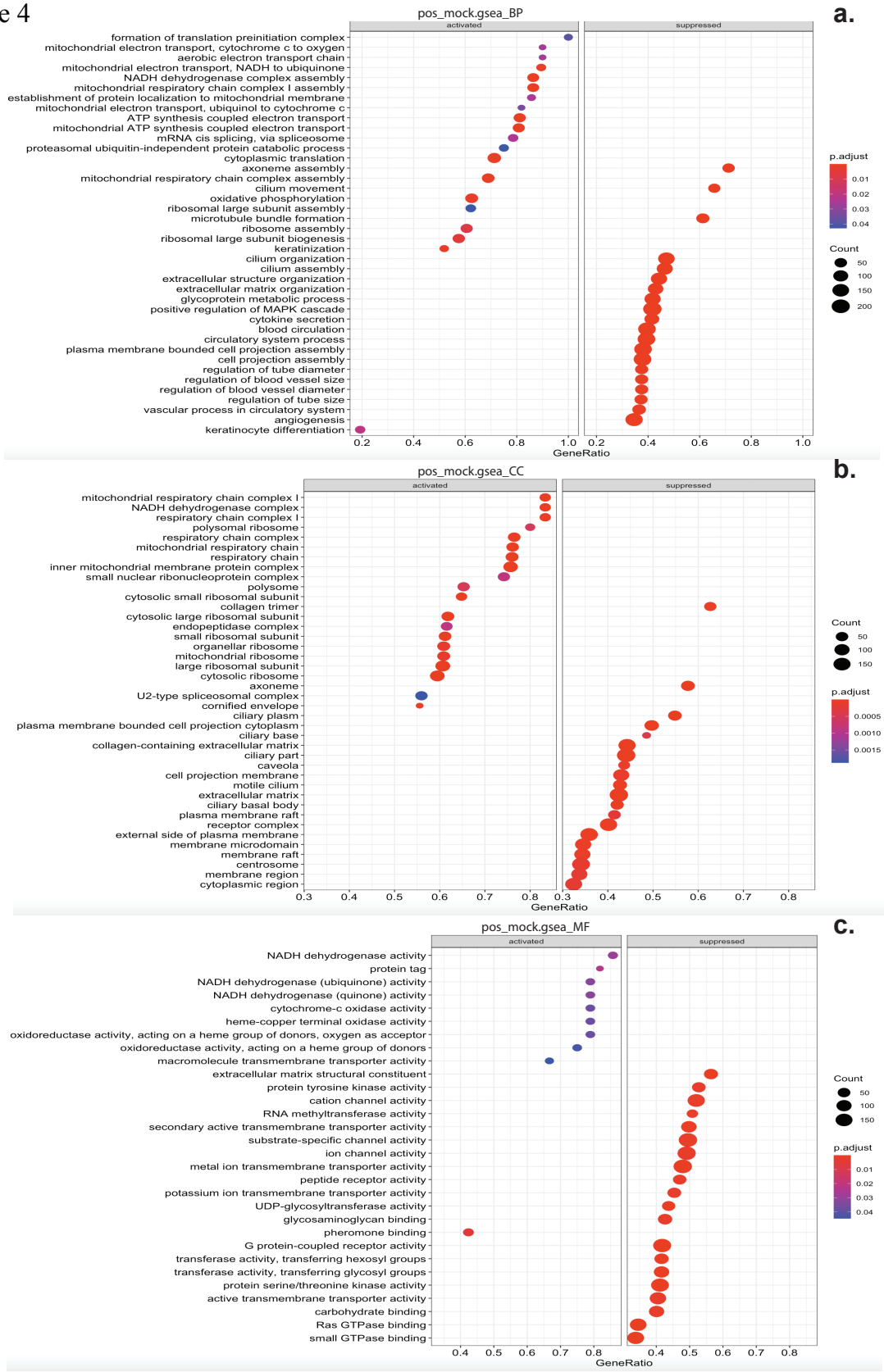

Extended Data Figure 5

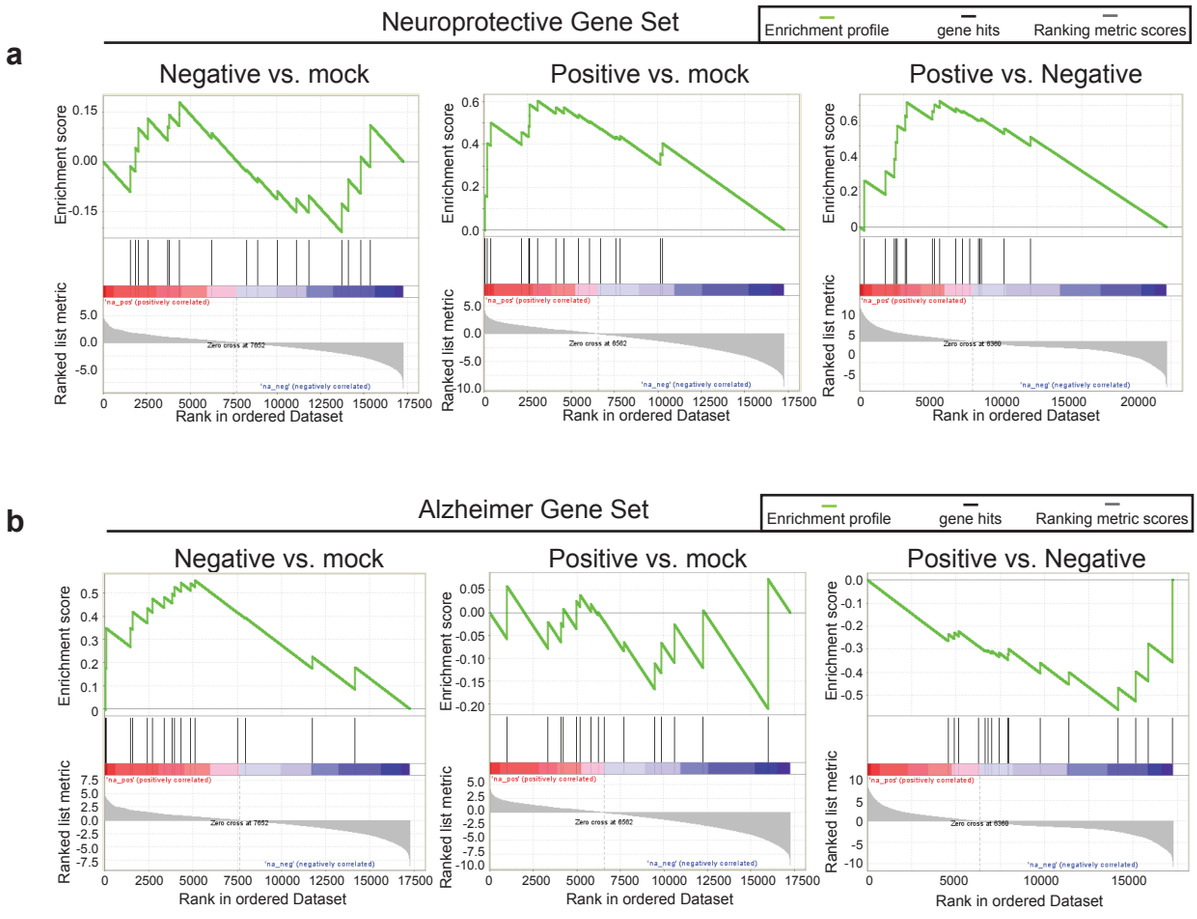

Extended Data Figure 6

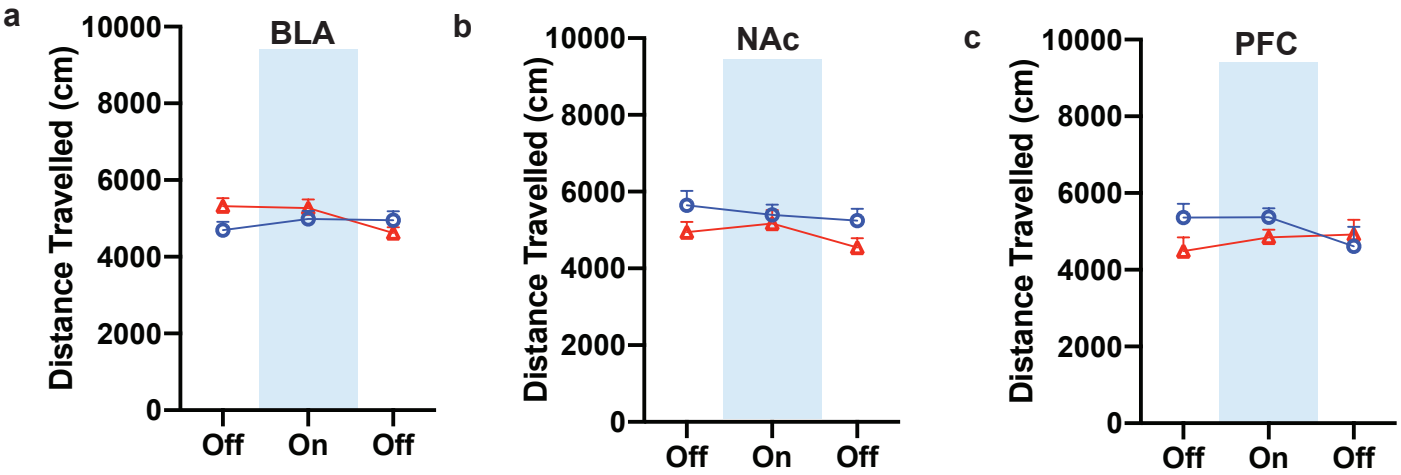

Extended Data Figure 7

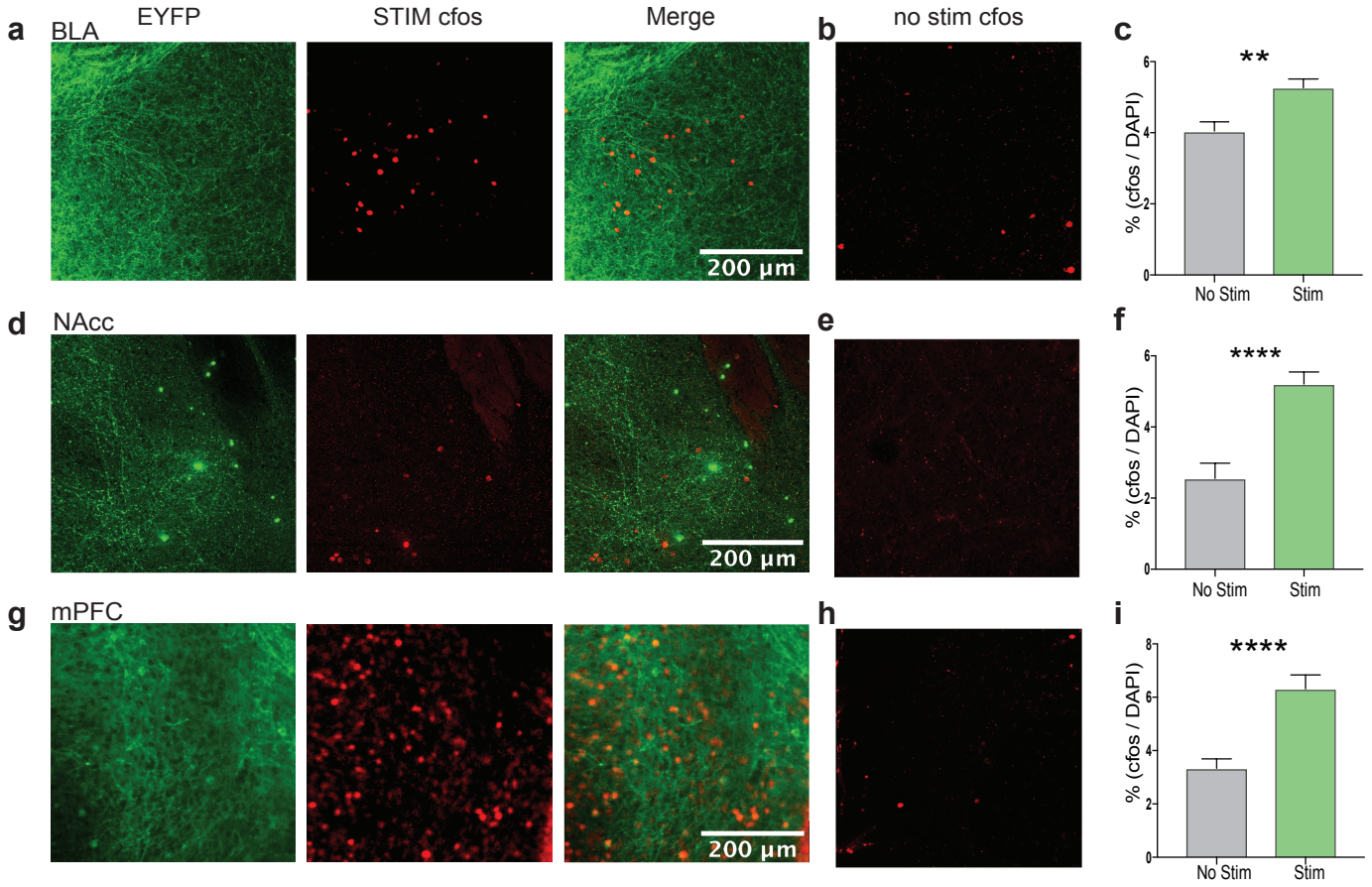

Extended Data Figure 8

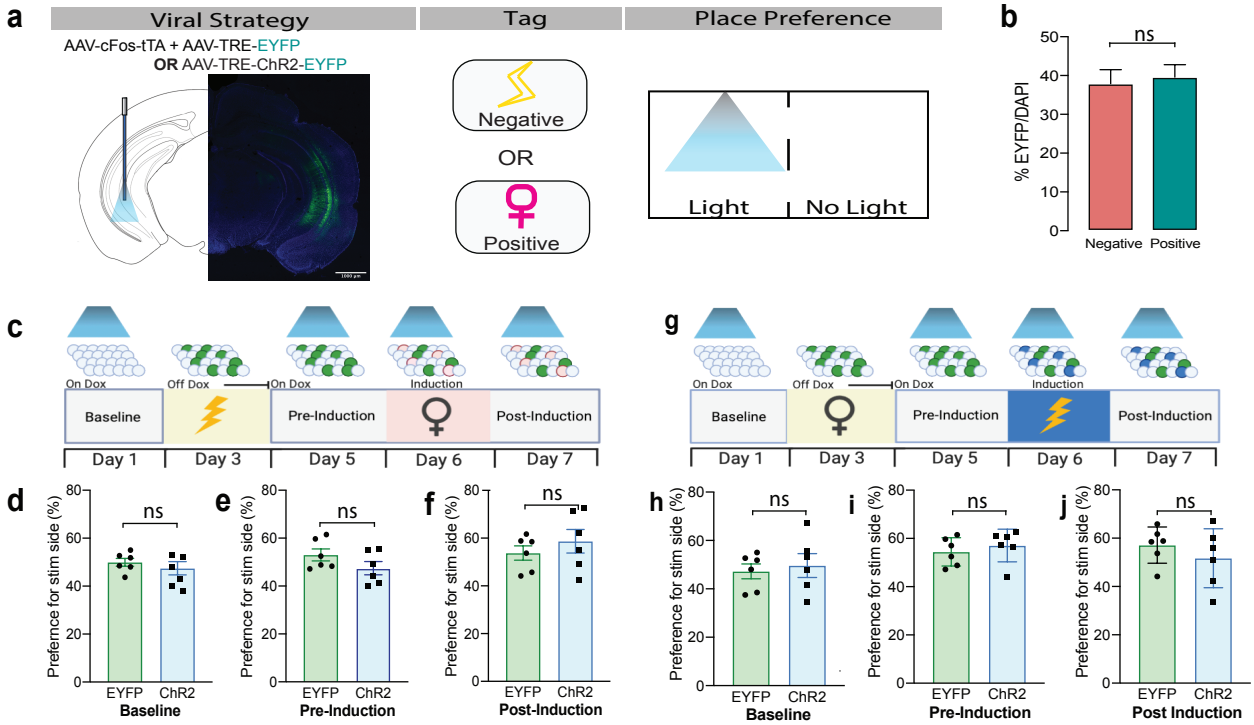

Extended Data Figure 9

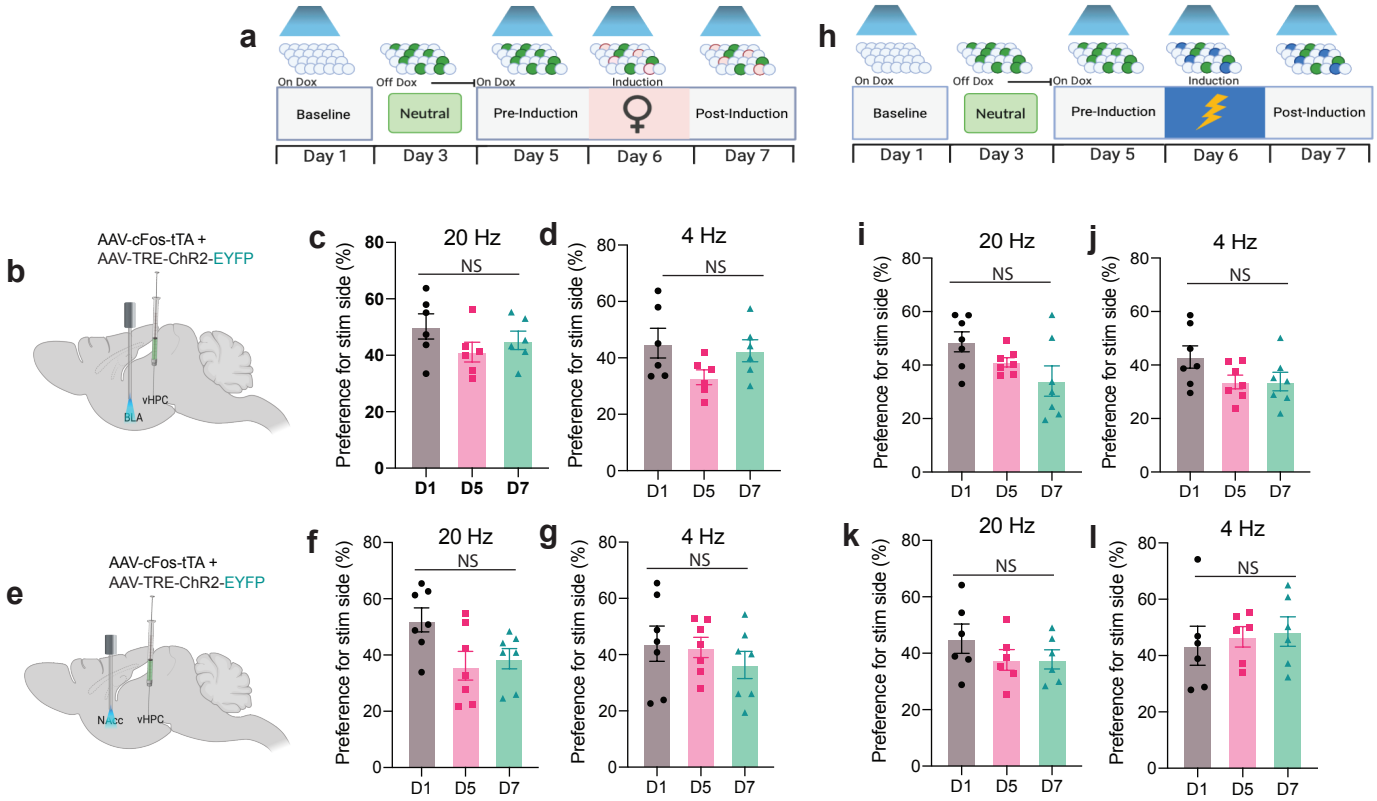

Table 1: Top up-regulated genes in positive tag

Gene Symbol	Gene Name
Neu1	Neuraminidase 1
Nefl	Neurofilament Light
Rab12	RAB12, Member RAS Oncogene Family
Hprt	Hypoxanthine Phosphoribosyltransferase 1
Il1b	Interleukin 1 Beta
Jpt2	Jupiter Microtubule Associated Homolog 2
Cxxc1	CXXC Finger Protein 1
Slc2a5	Solute Carrier Family 2 Member 5
Spp1	Secreted Phosphoprotein 1
Paxip1	PAX Interacting Protein 1
Abi3	ABI Family Member 3

Table 2: Top upregulated genes in negative tagged cells

Gene Symbol	Gene Name
Tmem144	Transmembrane Protein 144
Prox1	Prospero Homeobox 1
Pcdh9	Protocadherin 9
Rbbp9	RB Binding Protein 9, Serine Hydrolase
Fam76a	Family With Sequence Similarity 76 Member A
Frmd5	FERM Domain Containing 5
Fam234b	Family With Sequence Similarity 234 Member B
Bud23	BUD23 RRNA Methyltransferase And Ribosome Maturation Factor
Rpap2	RNA Polymerase II Associated Protein 2
Atl1	Atlastin GTPase 1
Btrc	Beta-Transducin Repeat Containing E3 Ubiquitin Protein Ligase
Eri1	Exoribonuclease 1
Pou3f1	POU Class 3 Homeobox 1
Pramef8	PRAME Family Member 8
Amph	Amphiphysin
Itgb1bp1	Integrin Subunit Beta 1 Binding Protein 1
Il1rap	Interleukin 1 Receptor Accessory Protein
Trim13	Tripartite Motif Containing 13
Insc	INSC Spindle Orientation Adaptor Protein

Table 3: Neuroprotective gene set

Gene Symbol	Gene Name
BDNF	Brain Derived Neurotrophic Factor
ACHE	Acetylcholinesterase
COLQ	Collagen Like Tail Subunit Of Asymmetric Acetylcholinesterase
MT-ND2	Mitochondrially Encoded NADH:Ubiquinone Oxidoreductase Core Subunit 2
SELENOW	Selenoprotein W
PINK1	PTEN Induced Kinase 1
CRYAB	Crystallin Alpha B
NRSN1	Neurensin 1
PTGDS	Prostaglandin D2 Synthase
LPAR1	Lysophosphatidic Acid Receptor 1
QDPR	Quinoid Dihydropteridine Reductas
PEA15A	Proliferation And Apoptosis Adaptor Protein 15
AKTIP	AKT Interacting Protein
GMFB	Glia Maturation Factor Beta
MAOA	Monoamine Oxidase A
BAG1	BAG Cochaperone 1
BNIP2	BCL2 Interacting Protein 2
TNFAIP6	TNF Alpha Induced Protein 6

Table 4: Neurodegenerative gene set

Gene Symbol	Gene Name
SPP1	Secreted Phosphoprotein 1
TTR	Transthyretin
C1QB	Complement C1q B Chain
CTSS	Cathepsin S
EGR1	Early Growth Response 1
GSN	Gelsolin
ADAM9	ADAM Metallopeptidase Domain 9
CTSD	Cathepsin D
CTSB	Cathepsin B
ARL6IP1	ADP Ribosylation Factor Like GTPase 6 Interacting Protein 1
CST3	Cystatin C
APP	Amyloid Precusor Protein
PSAP	Prosaposin
APOE	Apolipoprotein E
SLC1A3	Solute Carrier Family 1 Member 3
ENPP1	Ectonucleotide Pyrophosphatase/Phosphodiesterase 1